IEEE Access
Multidisciplinary ⋮ Rapid Review ⋮ Open Access Journal

Received 9 September 2022, accepted 20 September 2022, date of publication 28 September 2022, date of current version 7 October 2022.

Digital Object Identifier 10.1109/ACCESS.2022.3210540

RESEARCH ARTICLE

Machine Learning Based Self-Balancing and Motion Control of the Underactuated Mobile Inverted Pendulum With Variable Load

ALI UNLUTURK[1] **AND OMER AYDOGDU**[2]
[1]Electrical and Electronic Engineering Department, Faculty of Engineering and Architecture, Erzurum Technical University, 25050 Erzurum, Turkey
[2]Department of Electrical and Electronic Engineering, Faculty of Engineering and Natural Sciences, Konya Technical University, 42250 Konya, Turkey

Corresponding author: Ali Unluturk (ali.unluturk@erzurum.edu.tr)

ABSTRACT In this paper, a novel Machine Learning (ML) based Adaptive Fuzzy Logic-Proportional Integral (AFL-PI) controller was developed for the self-balancing and precision motion control of a two wheeled Underactuated-Mobile Inverted Pendulum (U-MIP) under variable payloads. One of the external disturbances in balance and motion control of the U-MIP is the amount of payload it carries on. To investigate the effectiveness of the proposed controller, a load bar was mounted on top of the U-MIP. The weights of 55gr each can be attached to this bar for variable payloads. The weights on the bar were labeled as three different classes: Low Load (LL), Normal Load (NL) and Heavy Load (HL). Artificial Neural Network (ANN), Linear Discriminant Analysis (LDA), Support Vector Machine (SVM) and k-Nearest Neighbors (k-NN) models were tested to obtain the highest payload class estimation. The highest load classification accuracy was achieved with ANN. Therefore, the ANN model was applied on the U-MIP. The balance performance of the U-MIP was compared by applying the classical FL-PI and ANN based AFL-PI controller on the robot. In order to compare the body tilt angle performance of the U-MIP, the optimal FL-PI parameter in LL was applied for NL and HL conditions without changing. Then, the proposed ANN based AFL-PI controller was implemented on U-MIP. With the proposed novel controller, the body tilt angle variation of the U-MIP was improved by %29.42 for NL and %55.62 for HL compared to the classical FL-PI controller. The validity of the proposed controller was proved by real experiments.

INDEX TERMS Machine learning, adaptive fuzzy logic control, balance robot, sensor fusion.

I. INTRODUCTION

In recent years, technology has developed rapidly and has become an indispensable part of our lives. It has also led to the development of many robotic tools that make our lives easier. Various personal vehicles that can move flexibly and offer ease of access in narrow places have been used in many areas such as city centers, shopping malls, hospitals, etc. [1], [2], [3], [4], [5], [6], [7]. Segways, one of the most well-known and with extraordinary capabilities, have been actively used in shopping centers, hospitals, airports, factories and many areas to transport people from one place to another. Two wheeled vehicles are widely preferred in many fields due to their advantages such as small footprint, flexible mobility and simple mechanism. Two wheeled self-balancing robots, which is different form of the inverted pendulum system, has a nonlinear structure with Single Input Multi Output (SIMO) controller [8]. Due to nonlinear structure and challenging control characteristics, the self-balancing and motion control of this robotic system is very difficult. In addition, ground robots, which can move quickly and overcome indoor obstacles, often lack speed or versatility in maneuvering [9]. Hence, it has attracted a remarkable attention of many researchers who have been doing theoretical and applied studies in the field of robotics. There have been many studies to solve this robot equilibrium and motion control problem using various control techniques in the literature. Nonlinear control structures with different analyses and designs [10], [11] dual-mode model predictive control [12], vision-based adaptive control [13], Sliding Mode Control

The associate editor coordinating the review of this manuscript and approving it for publication was Okyay Kaynak.

(SMC) [14], adaptive fuzzy control [15], Takagi-Sugeno type Fuzzy Logic Control (FLC) [16], interval Type-2 FLC [17], semiconcave Control Lyapunov Function (CLF) [18] and advanced interval Type-2 Fuzzy SMC [19] are some of them. Over the past decades, Machine Learning (ML) and Fuzzy Logic (FL) based intelligent control systems have been a dominant topic in research, robotics or control societies. Because, ML and FL based hybrid intelligent controllers offer a robust nonlinear controller for complicated systems with dynamic uncertainties and functional uncertainty as well as disturbances [16], [19]. The Fuzzy Logic Controllers (FLCs) have been extensively used and successfully applied in control problem of robotic systems where its mathematical model is difficult to obtain. On the other hand, FLCs cannot assure the global stability of the closed loop system for nonlinear complex systems with uncertainties [20]. The ML is considered as a subfield Artificial Intelligence (AI) [21]. It is about extracting knowledge from data [22]. Data are used to estimate or reply to future data [23]. ML algorithms are widely used in tasks such as automatic detection of objects in images (a crucial component of driver-assisted and self-driving cars), speech recognition (which power voice command technology), knowledge discovery in medical sciences (used to improve our understanding of complex diseases) and predictive analytics (leveraged for sales and economic forecasting) [24]. Many techniques and methodologies for ML tasks have been developed in progress of time [21]. ML algorithms that learn from input/output data pairs are called supervised learning algorithms [23]. The Artificial Neural Network (ANN), Linear Discriminant Analysis (LDA), Support Vector Machine (SVM) and k-Nearest Neighbours (k-NN) are one of the supervised machine learning approaches [25]. In the recent times, many researchers have combined the FLCs with machine learning methods [26], [27].

Nonlinear dynamics that cannot be modeled and a tendency to instability due to its structure are important features of the U-MIP robot. In addition, the most crucial issue in U-MIP control is how to handle parametric, unmodeled dynamics, and environmental disturbances [28]. The amount of payload that the U-MIP carries on is one of the external disturbances that negatively affect its ability to maintain self-balance and motion control. However, the reference body tilt angle is very important in the self-balancing and stable motion control of the U-MIP. The controller parameter should be changed in accordance with the payload the U-MIP carries to maintain its self-balance and perform the desired motions. Besides, as the amount of payload on the U-MIP increases, optimum reference body tilt angle should be determined according to the payload for stable motion control. Classical control techniques cannot adapt to the parameter changes of the system. Hence, these controllers are insufficient for stable motion control under variable payload of the U-MIP. Robots such as U-MIP have operational payload capacities according to their mechanical structures. Considering the electromechanical system components of the U-MIP, the total payload was determined to be 495gr. The 495gr payload on the U-MIP was grouped as Low Load ($0 < LL \leq 165$gr), Normal Load ($165 < NL \leq 330$gr) and Heavy Load ($330 < HL \leq 495$gr). These three main payload categories were predicted using ML based classifiers and data obtained from the U-MIP robot. To estimate variable payloads, ML methods such as ANN, LDA, SVM, and k-NN were used in this study. The best results in real-time payload forecast were obtained using ANN. For use in ANN based payload estimation, the robot's body tilt angle change, the linear displacement of the wheels and the controller output (voltage applied to the motors) data were obtained. Then, new features such as Mean Absolute Target Tilt Angle Deviation Error (MATTADE), Mean Absolute Target Linear Displacement Error (MATLDDE) and Mean Absolute Target Controller Output Deviation Error (MATCODE) were extracted from robot data. The effectiveness of the proposed ML based AFL-PI control was tested under variable payload and proved to be highly robustness against uncertainties.

The topics discussed in the article are as follows. In section II, we describe the mechanical design, hardware and Inertial Measurement Unit (IMU) of the U-MIP. In section III, a revised mathematical modelling of the U-MIP is derived. The developed ANN based AFL-PI control scheme is given in section IV. In section V, real-time performance evaluation of the proposed ANN based AFL-PI controller is presented under variable payload. In the last section, the proposed ANN based AFL-PI controller are interpreted and evaluated.

II. ROBOT OVERVIEW

A. HARDWARE OF THE U-MIP

The overview of the hardware components of the U-MIP robot is seen in Fig. 1. On the U-MIP, two 6.25 cm radius wheels are mounted on Permanent Magnet Direct Current (PMDC) motors with gearboxes. PMDC motors used for the motion of the robot have incremental encoders. It also has a Lithium Polymer (Li-Po) battery, a Cortex M3-based microcontroller, VNNH5019 PMDC motor driver board with dual channel, an HC-05 bluetooth unit, and a 9-DoF BNO055 IMU.

B. INERTIA MEASUREMENT UNIT

Figure 1 shows the U-MIP robot control circuit board that we designed, which includes the BNO055 IMU.

The BNO055 IMU was used to measure the tilt angle, which is very important for the U-MIP's self-balancing and motion control. The 3 DoF accelerometer sensor in the structure of this BNO055 IMU is adjusted to ± 4g sensitivity, while the gyroscope sensor 3 DoF is adjusted to $\pm 250^\circ/$s. In addition, BNO055 IMU has 3-axis magnetometer sensor. With the sensor groups on the IMU, measurements can be taken in three axes. The BN0055 was connected to the microcontroller via the I2C. The gyroscope in the hardware system measures the angular velocity of the robot, in other words, the rate of change in the orientation of the robot. These sensors contain

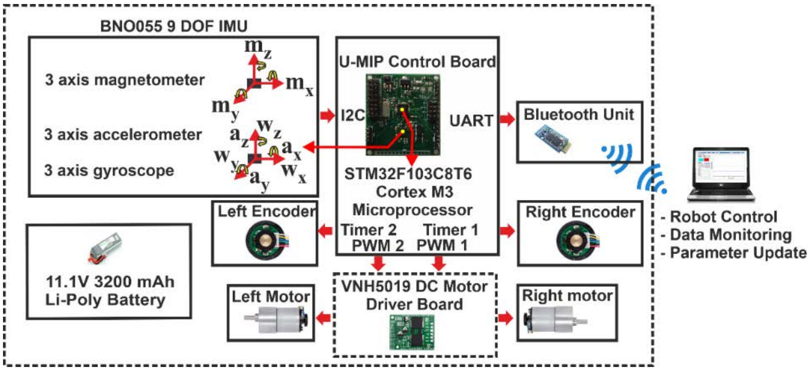

FIGURE 1. Hardware block diagram of the U-MIP.

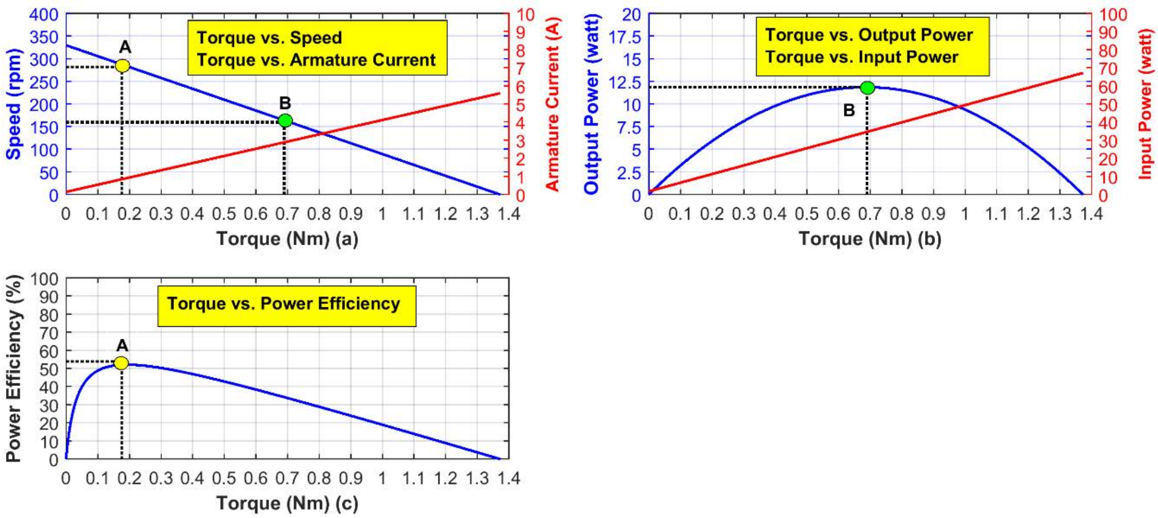

FIGURE 2. Characteristics curves of the PMDC motor used in U-MIP.

some noise sources in their structure. The main noise sources in the gyroscope sensor are quantization noise, bias and angle random walk [29]. The acceleration sensor generates a high noise signal at the smallest vibrations [30]. In order to get accurate measurement from these sensors, the sensors must be calibrated. Also, sensor fusion algorithms are required. The BNO055 9-axis absolute orientation IMU we used in the study was calibrated by the manufacturer and an embedded sensor fusion algorithm [31].

III. DYNAMIC MODELLING OF THE U-MIP

Determining of the parameters are important while obtaining the mathematical model of U-MIP robot. Table 1 shows the parameters of the revised U-MIP [32], [33]. One of the most important components in the U-MIP robot is the actuators. PMDC motor is preferred as the actuator in the U-MIP robot. In Fig. 2, the characteristics curves of the PMDC motor at 12V were obtained by using the document in [34]. The basic equations of Fig. 2(a), (b), (c) are as follows, respectively.

$$n_{shaft} = \frac{60V_t}{2\pi K_e} - \frac{60R_a}{2\pi K_t K_e}\tau_{out} \tag{1}$$

$$P_{out} = \frac{V_t}{K_e}\tau_{out} - \frac{R_a}{K_t K_e}\tau_{out}^2 \tag{2}$$

$$\%\eta = \left(\frac{\omega_{shaft}}{V_t I_a}\tau_{out} - \frac{\omega_{shaft}}{V_t I_a}\tau_{fr}\right) \times 100 \tag{3}$$

where, n_{shaft} speed of the motor shaft in revolution per minute, τ_{out} output torque, P_{out} output power, $\%\eta$ percentage of efficiency. In detail, how the equations are obtained can be examined in detail from reference [35].

In Fig. 2(a), slope of torque versus armature current is the current constant K_c. It is obtained as

$$K_c = \frac{I_{sec} - I_{nl}}{\tau_{set} - 0} = \frac{5.5 - 0.2}{1.3734} = 3.86\ \mathrm{A}/\mathrm{Nm} \tag{4}$$

The reciprocal of this slope (torque constant) is given as

$$K_t = \frac{1}{K_c} = \frac{1}{3.86} = 0.26\ \mathrm{Nm}/\mathrm{A} \tag{5}$$

The motor friction torque τ_{fr} is determined multiplying the K_t and I_{nl}.

$$\tau_{fr} = K_t I_{nl} = \frac{(0.26\mathrm{Nm})(0.2\mathrm{A})}{\mathrm{A}} = 0.052\mathrm{Nm} \tag{6}$$

Since the inductance of the PMDC motor (L_m) is very small, it can be considered as zero. In addition, friction coefficient

TABLE 1. Physical parameters of U-MIP [32], [33].

Symbol	Quantity	Value
V_{nl}	rated voltage	12 V
n_{nl}	no load speed	330 rpm
ω_{max}	Maximum angular speed for stable motion of in LL, NL, HL	23 rad/sec
V_{max}	Maximum linear speed for stable motion of LL, NL, HL	1.44 m/sec
I_{nl}	no load current	0.2 A
n_{me}	speed at maximum η	280 rpm
I_{me}	current at maximum η	0.78 A
τ_{me}	torque at maximum η	0.18 Nm
P_{me}	output power at maximum η	5.1 W
P_{mp}	motor maximum output power	12 W
τ_{set}	stall extrapolation motor torque	1.3734 Nm
I_{sec}	stall extrapolation motor current	5.5 A
J_m	motor inertia moment	10^{-5} kgm^2
R_a	motor resistance	2.18 Ω
K_e	motor back EMF constant	0.33Vsec/rad
K_t	motor torque constant	0.26 Nm/A
f_m	friction coefficient between body and motor	0.0022
n	motor gear ratio	N_2:N_1=30:1
g	gravity acceleration	9.81 m/sec^2
m	wheel weight	0.146 kg
R	wheel radius	0.0625 m
J_w	wheel inertia moment	0.00029 kgm^2
M	body own weight (with screw load bar and bar nuts)	1.468 kg
m_{tp}	total payload of the U-MIP	0.495 kg
w	U-MIP body width	w=0.28 m
D	U-MIP body depth	D=0.16 m
H	U-MIP body height (with screw load bar)	H=0.31 m
J_ψ	body tilt inertia moment	0.012 kgm^2
J_ϕ	body yaw inertia moment	0.013 kgm^2

between wheel and floor of the U-MIP is considered to be zero. In addition, the friction coefficient between body and PMDC motor is given in Table 1. Terminal voltage on PMDC can be calculated as

$$V_t = I_a R_a + E_a \tag{7}$$

where I_a is armature current, R_a is armature resistance and E_a represents back-Electro Motor Force (back-EMF). If the armature current is $I_a = I_{sec}$ then $E_a = 0$, R_a can be determined as

$$R_a = \frac{V_n}{I_{sec}} = \frac{12V}{5.5A} = 2.18\Omega \tag{8}$$

The back-EMF is expressed as

$$E_a = K_e \omega_m \tag{9}$$

Voltage at no load of the motor described as

$$V_{nl} = I_{nl} R_a + K_e \omega_{nl} \tag{10}$$

Considering (7) and Table 1, the K_e value is approximately 0.33 Vsec/rad.

U-MIP system was modelled basing on Lagrangian method referred as Yaurihiso Yamamoto [33]. Coordinate systems and variables of U-MIP are depicted in Fig. 3. When U-MIP has a screw load bar, the distance between the floor and the top of the load bar is 38 cm.

In Fig. 3(a); θ_l and θ_r defines left and right wheel angle on coordinate system, θ denotes the average angle of left and right wheel, $\omega_m = \dot{\theta}$ denotes the average angular velocity of left and right wheel, ψ defines the body tilt angle. Fig. 3(b), (c) shows coordinate system of side and top views of U-MIP. In Fig. 3(b), (c); x_b, y_b, z_b denotes the system's center of gravity x_m, y_m, z_m denotes the robot wheel's center of gravity. The total payload carrying capacity of U-MIP is $m_{tp} = 0.495$kg. θ_{mr} and θ_{ml} denote the right and left wheel PMDC motor angle. In addition, the motion and self-balance control of the U-MIP are active between $-30° \leq \psi \leq 30°$. The body yaw angle is denoted by ϕ.

The displacement of the left and right wheels along the x-axis are defined as

$$X_L = \theta_l R \tag{11}$$

$$X_R = \theta_r R \tag{12}$$

The variation of (x_m, y_m, z_m), which is the center of gravity of the wheels of the U-MIP, are defined as

$$x_m = R\theta \cos\phi \tag{13}$$

$$y_m = R\theta \sin\phi \tag{14}$$

$$z_m = R \tag{15}$$

The mathematical equations of the U-MIP are obtained by the Lagrangian method considering the coordinate system in Fig. 3(b), (c). If x-axis of the U-MIP robot is positive direction at t = 0. Each coordinates are given as the following [33].

$$(\theta, \phi) = \left(\frac{1}{2}(\theta_l + \theta_r), \frac{R}{w}(\theta_r - \theta_l)\right) \tag{16}$$

$$(\dot{x}_m, \dot{y}_m) = (R\dot{\theta}\cos\phi, R\dot{\theta}\sin\phi) \tag{17}$$

$$(x_l, y_l, z_l) = \left(x_m - \frac{w}{2}\sin\phi, y_m + \frac{w}{2}\cos\phi, z_m\right) \tag{18}$$

$$(x_r, y_r, z_r) = \left(x_m + \frac{w}{2}\sin\phi, y_m - \frac{w}{2}\cos\phi, z_m\right) \tag{19}$$

$$(x_b, y_b, z_b) = \begin{pmatrix} x_m + L\sin\psi\cos\phi, \\ y_m + L\sin\psi\sin\phi, z_m + L\cos\psi \end{pmatrix} \tag{20}$$

The Lagrangian L is defined in (21).

$$L = T_1 + T_2 - U \tag{21}$$

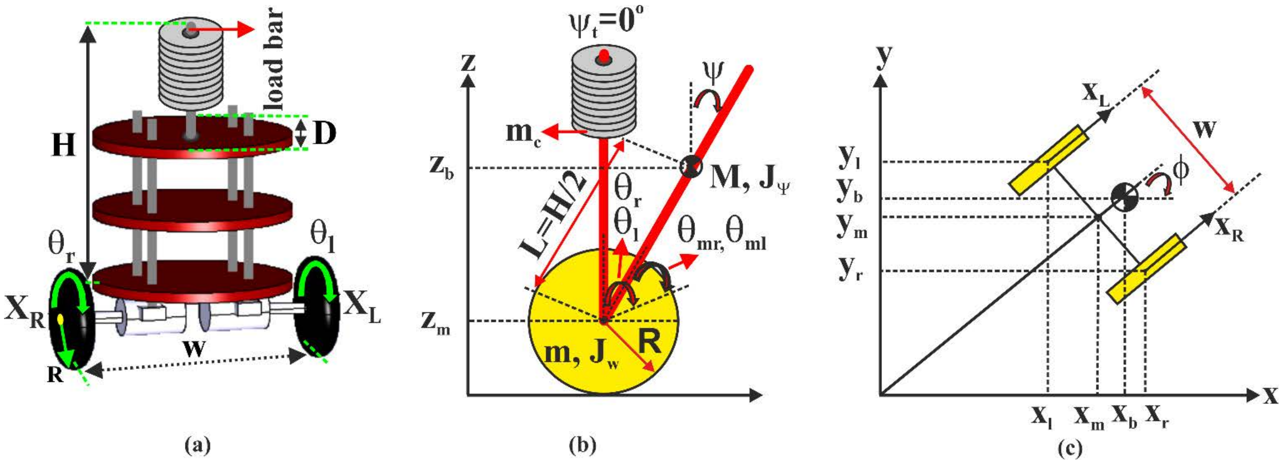

FIGURE 3. a) U-MIP b) side view of the U-MIP c) top view of the U-MIP.

where T_1 is translational kinetic energy, T_2 is rotational kinetic energy, and U is potential energy. U, T_1 and T_2 are given as

$$U = mgz_l + mgz_r + Mgz_b \tag{22}$$

$$T_1 = \frac{1}{2}m\left(\dot{x}_l^2+\dot{y}_l^2+\dot{z}_l^2\right)+\frac{1}{2}m\left(\dot{x}_r^2+\dot{y}_r^2+\dot{z}_r^2\right) + \frac{1}{2}M\left(\dot{x}_b^2+\dot{y}_b^2+\dot{z}_b^2\right) \tag{23}$$

$$T_2 = \frac{1}{2}J_w\dot{\theta}_l^2+\frac{1}{2}J_w\dot{\theta}_r^2+\frac{1}{2}J_\psi\dot{\psi}^2+\frac{1}{2}J_\phi\dot{\phi}^2 + \frac{1}{2}n^2J_m\left(\dot{\theta}_l-\dot{\psi}\right)^2+\frac{1}{2}n^2J_m\left(\dot{\theta}_r-\dot{\psi}\right)^2 \tag{24}$$

Lagrange equations are defined as

$$\frac{d}{dt}\left(\frac{\partial L}{\partial\dot{\theta}}\right)-\frac{\partial L}{\partial\theta}=F_\theta \tag{25}$$

$$\frac{d}{dt}\left(\frac{\partial L}{\partial\dot{\psi}}\right)-\frac{\partial L}{\partial\psi}=F_\psi \tag{26}$$

$$\frac{d}{dt}\left(\frac{\partial L}{\partial\dot{\phi}}\right)-\frac{\partial L}{\partial\phi}=F_\phi \tag{27}$$

From equations (25), (26) and (27) generalized forced equations are obtained as

$$\left[(2m+M)R^2+2J_w+2n^2J_m\right]\ddot{\theta} + \left(MLR\cos\psi-2n^2J_m\right)\ddot{\psi}-MLR\dot{\psi}^2\sin\psi=F_\theta \tag{28}$$

$$\left(MLR\cos\psi-2n^2J_m\right)\ddot{\theta}+\left(ML^2+J_\psi+2n^2J_m\right)\ddot{\psi} - MgL\sin\psi-ML^2\dot{\phi}^2\sin\psi\cos\psi=F_\psi \tag{29}$$

$$\left[\frac{1}{2}mw^2+J_\phi+\frac{w^2}{2R^2}\left(J_w+n^2J_m\right)+ML^2\sin^2\psi\right]\ddot{\phi} + 2ML^2\dot{\psi}\dot{\phi}\sin\psi\cos\psi=F_\phi \tag{30}$$

Considering the PMDC motor torque and viscous friction, the generalized forces can be rearranged as

$$\left(F_\theta,F_\psi,F_\phi\right)=\left(F_l+F_r,F_\psi,\frac{w}{2R}\left(F_r-F_l\right)\right) \tag{31}$$

$$F_l = nK_tI_{al}+f_m\left(\dot{\psi}-\dot{\theta}_l\right)-f_w\dot{\theta}_l \tag{32}$$

$$F_r = nK_tI_{ar}+f_m\left(\dot{\psi}-\dot{\theta}_l\right)-f_w\dot{\theta}_r \tag{33}$$

$$F_\psi = -nK_tI_{al}-nK_tI_{ar}-f_m\left(\dot{\psi}-\dot{\theta}_l\right)-f_m\left(\dot{\psi}-\dot{\theta}_r\right) \tag{34}$$

where I_{al}, I_{ar} are the left and right PMDC motor current. Since the PMDC motor is drived by the Pulse Wide Modulation (PWM) technique, the generalized forces must be written depending on the voltage applied to the left (V_{tl}) and right (V_{tr}) wheels. I_{al}, I_{ar} are defined as

$$I_{al}=\frac{V_{tl}+K_e\left(\dot{\psi}-\dot{\theta}_l\right)}{R_a},\quad I_{ar}=\frac{V_{tr}+K_e\left(\dot{\psi}-\dot{\theta}_r\right)}{R_a} \tag{35}$$

Generalized forces depending on the motor voltage is given as

$$F_\theta = \alpha\left(V_{tl}+V_{tr}\right)-2\left(\beta+f_w\right)\dot{\theta}+2\beta\dot{\psi} \tag{36}$$

$$F_\psi = -\alpha\left(V_{tl}+V_{tr}\right)+2\beta\dot{\theta}-2\beta\dot{\psi} \tag{37}$$

$$F_\phi = \frac{w}{2R}\alpha\left(V_{tr}-V_{tl}\right)-\frac{w^2}{2R^2}\left(\beta+f_w\right)\dot{\phi} \tag{38}$$

$$\alpha=\frac{nK_t}{R_a},\quad \beta=\frac{nK_tK_e}{R_a}+f_m \tag{39}$$

State space equations are obtained by linearizing the equations of motion around the equilibrium point of the U-MIP. Briefly, the ψ value around the equilibrium point of the U-MIP is quite close to 0. Hence $\sin\psi \cong \psi$ and $\cos\psi \cong 1$. At the same time, quadratic terms are omitted. Under these conditions, the equations of motion (28), (29) and (30) are rearranged as

$$\left[(2m+M)R^2+2J_w+2n^2J_m\right]\ddot{\theta} + \left(MLR-2n^2J_m\right)\ddot{\psi}=F_\theta \tag{40}$$

$$\left(\mathrm{MLR}-2\mathrm{n}^2\mathrm{J_m}\right)\ddot{\theta}+\left(\mathrm{ML}^2+\mathrm{J}_\psi+2\mathrm{n}^2\mathrm{J_m}\right)\ddot{\psi}-\mathrm{MgL}\psi=\mathrm{F}_\psi \tag{41}$$

$$\left[\frac{1}{2}\mathrm{mw}^2+\mathrm{J}_\phi+\frac{\mathrm{w}^2}{2\mathrm{R}^2}\left(\mathrm{J_w}+\mathrm{n}^2\mathrm{J_m}\right)\right]\ddot{\phi}=\mathrm{F}_\phi \tag{42}$$

The generalized equations F_θ and F_ψ discussed in the article can be expressed as

$$\mathrm{E}\begin{bmatrix}\ddot{\theta}\\ \ddot{\psi}\end{bmatrix}+\mathrm{F}\begin{bmatrix}\dot{\theta}\\ \dot{\psi}\end{bmatrix}+\mathrm{G}\begin{bmatrix}\theta\\ \psi\end{bmatrix}=\mathrm{H}\begin{bmatrix}\mathrm{V_{tl}}\\ \mathrm{V_{tr}}\end{bmatrix} \tag{43}$$

E, F, G and H in (43),

$$\mathrm{E}=\begin{bmatrix}(2\mathrm{m}+\mathrm{M})\mathrm{R}^2+2\mathrm{J_w}+2\mathrm{n}^2\mathrm{J_m} & \mathrm{MLR}-2\mathrm{n}^2\mathrm{J_m}\\ \mathrm{MLR}-2\mathrm{n}^2\mathrm{J_m} & \mathrm{ML}^2+\mathrm{J}_\psi+2\mathrm{n}^2\mathrm{J_m}\end{bmatrix}$$

$$\mathrm{F}=2\begin{bmatrix}\beta+\mathrm{f_w} & -\beta\\ -\beta & \beta\end{bmatrix}$$

$$\mathrm{G}=\begin{bmatrix}0 & 0\\ 0 & -\mathrm{MgL}\end{bmatrix}$$

$$\mathrm{H}=\begin{bmatrix}\alpha & \alpha\\ -\alpha & -\alpha\end{bmatrix}$$

The state variable x_1 can be defined as

$$\mathrm{x}_1=\begin{bmatrix}\theta & \psi & \dot{\theta} & \dot{\psi}\end{bmatrix}^{\mathrm{T}},\quad \mathrm{u}=\begin{bmatrix}\mathrm{V_{tl}} & \mathrm{V_{tr}}\end{bmatrix}^{\mathrm{T}} \tag{44}$$

where u is system input. State-space model equation of the U-MIP can be expressed as

$$\dot{\mathrm{x}}_1=\mathrm{A}_1\mathrm{x}_1+\mathrm{B}_1\mathrm{u} \tag{45}$$

The matrix A_1 in the state-space model is defined as

$$\mathrm{A}_1=\begin{bmatrix}0 & 0 & 1 & 0\\ 0 & 0 & 0 & 1\\ 0 & \mathrm{A}_1(3,2) & \mathrm{A}_1(3,3) & \mathrm{A}_1(3,4)\\ 0 & \mathrm{A}_1(4,2) & \mathrm{A}_1(4,3) & \mathrm{A}_1(4,4)\end{bmatrix} \tag{46}$$

The matrix B_1 in the state space model is defined as

$$\mathrm{B}_1=\begin{bmatrix}0 & 0\\ 0 & 0\\ \mathrm{B}_1(3) & \mathrm{B}_1(3)\\ \mathrm{B}_1(4) & \mathrm{B}_1(4)\end{bmatrix} \tag{47}$$

The variables in the A_1 and B_1 matrix are defined as $A_1(3,2)=-gMLE(1,2)/\det(E)$

$$\begin{aligned}\mathrm{A}_1(4,2)&=\mathrm{gMLE}(1,1)/\det(\mathrm{E})\\ \mathrm{A}_1(3,3)&=-2\left[(\beta+\mathrm{f_w})\mathrm{E}(2,2)+\beta\mathrm{E}(1,2)\right]/\det(\mathrm{E})\\ \mathrm{A}_1(4,3)&=2\left[(\beta+\mathrm{f_w})\mathrm{E}(1,2)+\beta\mathrm{E}(1,1)\right]/\det(\mathrm{E})\\ \mathrm{A}_1(3,4)&=2\beta\left[\mathrm{E}(2,2)+\mathrm{E}(1,2)\right]/\det(\mathrm{E})\\ \mathrm{A}_1(4,4)&=-2\beta\left[\mathrm{E}(1,1)+\mathrm{E}(1,2)\right]/\det(\mathrm{E})\\ \mathrm{B}_1(3)&=\alpha\left[\mathrm{E}(2,2)+\mathrm{E}(1,2)\right]/\det(\mathrm{E})\\ \mathrm{B}_1(4)&=-\alpha\left[\mathrm{E}(1,1)+\mathrm{E}(1,2)\right]/\det(\mathrm{E}).\end{aligned}$$

The state space model of U-MIP without screw load bar and bar nuts (In this case, M=1.392 kg and H=0.09 m) is described as

$$\begin{bmatrix}\dot{\theta}\\ \dot{\Psi}\\ \ddot{\theta}\\ \ddot{\Psi}\end{bmatrix}=\begin{bmatrix}0 & 0 & 1 & 0\\ 0 & 0 & 0 & 1\\ 0 & 24.8141 & -52.0474 & 52.0474\\ 0 & 44.3049 & 75.0414 & -75.0414\end{bmatrix}\begin{bmatrix}\theta\\ \Psi\\ \dot{\theta}\\ \dot{\Psi}\end{bmatrix}+\begin{bmatrix}0 & 0\\ 0 & 0\\ 78.7130 & 78.7130\\ -113.4876 & -113.4876\end{bmatrix}\begin{bmatrix}\mathrm{V_{tl}}\\ \mathrm{V_{tr}}\end{bmatrix} \tag{48}$$

TABLE 2. Eigenvalues of the variable loaded U-MIP.

U-MIP's weight	Eigenvalues	
U-MIP's initial weight as 1.468kg	$\lambda_{1,1}=0$	$\lambda_{1,2}=5.2196$
	$\lambda_{1,3}=-5.1551$	$\lambda_{1,4}=-119.6527$
1.578 kg (LL) (added 110gr)	$\lambda_{2,1}=0$	$\lambda_{2,2}=5.2254$
	$\lambda_{2,3}=-5.1566$	$\lambda_{2,4}=-119.2739$
1.743 kg (NL) (added 275gr)	$\lambda_{3,1}=0$	$\lambda_{3,2}=5.2332$
	$\lambda_{3,3}=-5.1580$	$\lambda_{3,4}=-118.7121$
1.908 kg (HL) (added 440gr)	$\lambda_{4,1}=0$	$\lambda_{4,2}=5.2402$
	$\lambda_{4,3}=-5.1586$	$\lambda_{4,4}=-118.1574$

With the state space equations, it can be calculated that the system is completely controllable and observable. The open loop eigenvalues of the U-MIP with variable payload are given in Table 2.

With increasing payload, the positive eigenvalues in the right half plane leads the instability of the system. In order to stabilize the system under variable load, we need a controller that can carry the closed-loop eigenvalues of the system to the left half plane. The controller parameters were roughly determined by simulation results using the mathematical model of the U-MIP system under variable payload. Then, the controller parameters of the U-MIP under variable payloads were obtained by fine-tuning via real-time robot control interface.

IV. PROPOSED ML BASED AFL-PI CONTROLLER

In order that the U-MIP system remains stable under variable payload, the controller parameters must be variable. Also, in the precise motion control of the U-MIP system, the reference input signal must be dynamic according to the payload. Due to these requirements, different classification algorithms ANN, LDA, SVM and k-NN have been evaluated for the estimation of variable payloads in the U-MIP. ANN is a flexible mathematical model that can learn a system behavior using input and output datasets. ANN is used in many different fields of engineering thanks to its learning ability. An ANN usually has an input layer, a hidden layer and an output layer. While there are as many neurons as the number of inputs of the system in the input layer of the ANN, there are as many neurons as the desired output number in the output layer [36]. Most researchers have determined the

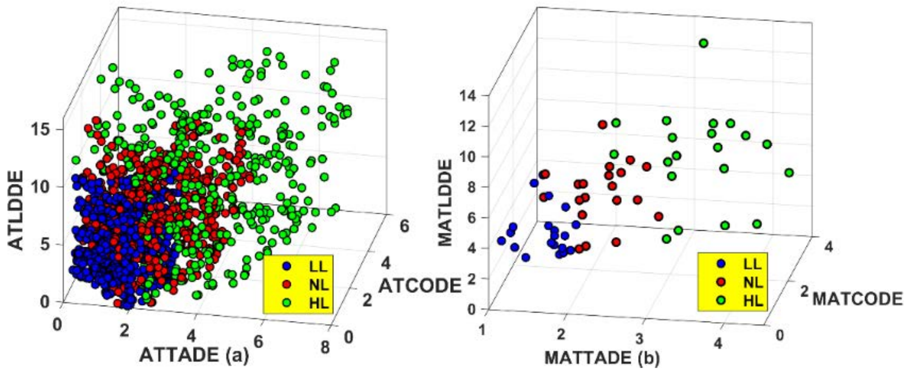

FIGURE 4. Distribution of a) new featured data b) the mean of new featured data (mean of each N=25 data).

number of neurons in the hidden layer by trial-and-error [37]. LDA is used as a tool for classification, dimension reduction, and data visualization. It is simplicity and provide robust, decent, and interpretable classification results [38]. SVM, proposed by Vapnik *et al.*, is a supervised machine learning approach [39]. SVM is a highly successful learning method in many applications. The origin of SVM is based on two basic ideas. The first approach is to use linear classifiers in this new space after mapping feature vectors in nonlinear high-dimensional space. The second assumption involves using wide-margin linear classifiers to maximally separate the data from the potentially infinite number of hyperplanes that can use [39], [40]. Nearest Neighbour (NN) is a machine learning algorithm that is resistant to old, simple and noisy training data. However, its performance is highly dependent on the quality of the training data [41]. Each new sample is compared to existing samples using a distance metric, and the nearest available sample is used to assign the class to the new one. Sometimes more than one NN is used and the majority class of the k-NN (or distance-weighted average if the class is numeric) is assigned to the new sample. This is called the k-NN method [39], [40], [41], [42]. The new dataset for classification is consisted of three features after feature extraction process. These new featured data are Absolute Target Tilt Angle Deviation Error (ATTADE), Absolute Target Linear Displacement Deviation Error (ATLDDE) and Absolute Target Controller Output Deviation Error (ATCODE). In Fig. 4(a), data distributions obtained for Low Load (LL), Normal Load (NL) and Heavy Load (HL) are shown. The average of these data was used in the ANN based payload estimation algorithm in the developed AFL-PI controller structure. MATTADE, MATLDDE and MATCODE data, which are used as input data of ANN, LDA, SVM and k-NN for load estimation, are defined as (49), (50) and (51).

$$\mathrm{MATTADE} = \frac{1}{\mathrm{N}}\sum_{1}^{\mathrm{N}} |\Psi_t - \Psi| \tag{49}$$

$$\mathrm{MATLDDE} = \frac{1}{\mathrm{N}}\sum_{1}^{\mathrm{N}} |X_t - X_d| \tag{50}$$

$$\mathrm{MATCODE} = \frac{1}{\mathrm{N}}\sum_{1}^{\mathrm{N}} |U_t - U_c| \tag{51}$$

Here, N = 25. Also, the sampling time of the data measurement from the U-MIP is 20msec. The target body tilt angle of the U-MIP is Ψ_t. The target displacement of the U-MIP refers to X_t. The controller output of the U-MIP when the robot is at the target body tilt angle refers to U_t. These reference target variables have a value of zero. The actual body tilt angle is Ψ. The actual linear displacement is X_d. The actual controller output is U_c. The distribution of the extracted data is given in Fig. 4(b). The highest load estimation performance was obtained with ANN, which is one of the machine learning algorithms used. The propose a novel ANN based AFL-PI controller is given in Fig 5. The FLC includes input normalization, fuzzification, fuzzy inference system, defuzzification and output normalization. The knowledge and skill of the expert in FLC design is the most important factor in the design.

In addition, the selection of the normalization factors of the input values and the denormalization of the output in the fuzzy controller design provide a general solution in the overall working space. Although normalization and denormalization parameters have linear characteristics, they are critical in fuzzy controller performance. While there is no payload on the robot, normalization parameter coefficients are defined as $K_1 = 0.3$, $K_2 = 0.65$, and denormalization parameter coefficient is chosen as $K_3 = 0.55$. The parameters were defined experimentally considering balance performance data obtained by robot control interface. The utilized triangular membership functions are used for input and output linguistic variables as Negative Big (NB), Negative Medium (NM), Negative Small (NS), Zero (Z), Positive Small (PS), Positive Medium (PM), Positive Big (PB). The performance of the FLC depends on the information and experience. Decision table is 7 × 7 and 49 fuzzy rule base was developed for this system. In general, Table 3 shows the fuzzy rules. IF-THEN rule base is defined linguistically by expert on the system. Mamdani method is used for ANN based AFL-PI control. Max-Min operation used for composition. The fuzzy inference mechanism is expressed as

$$\mu_i(u) = \max(\mu_i(e_1), \mu_i(e_2)) \tag{52}$$

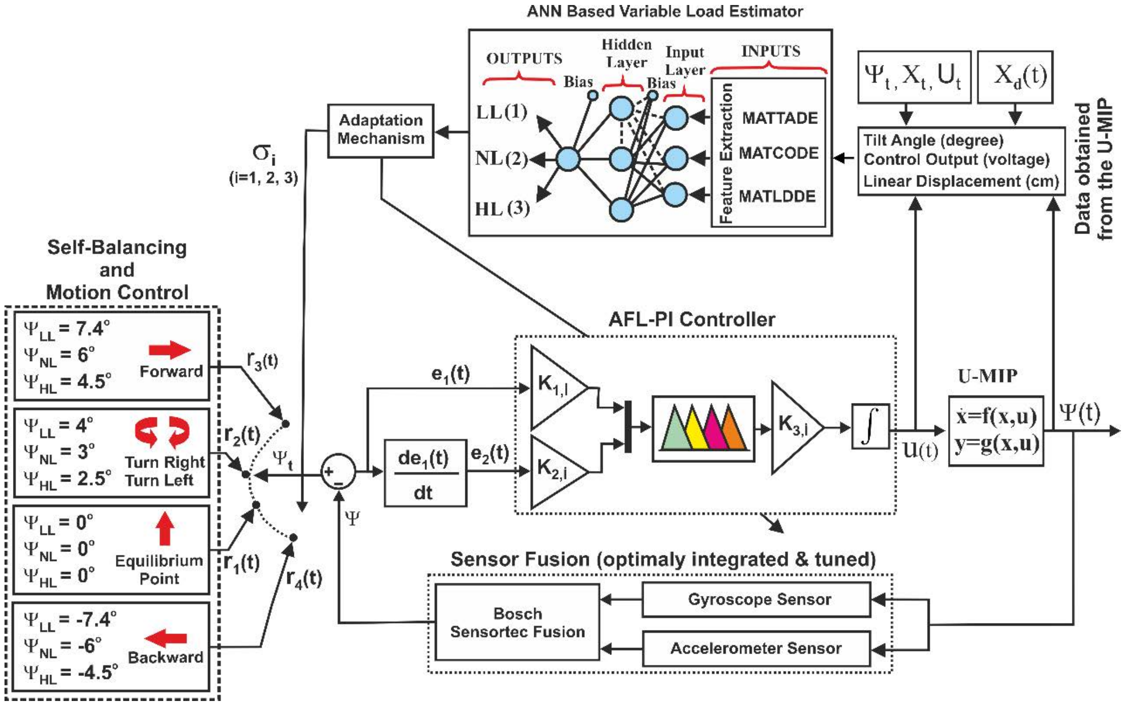

FIGURE 5. The structure of the proposed novel ANN based AFL-PI.

TABLE 3. Rule base of ANN based AFL-PI controller.

e_1	e_2						
	NB	**NM**	**NS**	**Z**	**PS**	**PM**	**PB**
NB	NB	NB	NB	NB	NM	NS	Z
NM	NB	NB	NB	NM	NS	Z	PS
NS	NB	NB	NM	NS	Z	PS	PM
Z	NB	NM	NS	Z	PS	PM	PB
PS	NM	NS	Z	PS	PM	PB	PB
PM	NS	Z	PS	PM	PB	PB	PB
PB	Z	PS	PM	PB	PB	PB	PB

The output in the form of the fuzzy set was converted to crisp values to produce the control signal of the U-MIP. This is called defuzzification. Finally, the output value was normalized in the opposite direction to produce the controller signal of the system. For the defuzzification process in this study, the commonly used center of gravity method was used.

According to this the control signal of U-MIP is given as

$$\Delta u = \frac{\sum_{j=1}^{m} d_j A(\mu_j)}{\sum_{j=1}^{m} A(\mu_j)} \tag{53}$$

where the fuzzy controller output is Δu. d_j is the distance between j^{th} fuzzy set and the center. $A(\mu_j)$ is the area value of j^{th} fuzzy set. As a result, the payload changes were estimated with the ANN adaptation mechanism and the controller parameters $K_{1,i}$, $K_{2,i}$ and $K_{3,i}$ were updated with the help of the switching function $\sigma_i (i = 1, 2, 3)$. The flow diagram of the proposed ANN based AFL-PI adaptation mechanism is given in Fig. 6.

As seen from the adaptation flowchart, firstly AFL-PI parameters and ANN classifier are started. Then, blocks A, B and C are run every 20ms. When ''ind'' variable reaches 499, block D is executed. Then, the adaptation mechanism performs and the PWM signals for the self-balance and motion control of the U-MIP are applied to the PMDC driver.

V. EXPERIMENTAL RESULTS

To analyze the stability of the U-MIP under varying load conditions, 55g masses were added one by one to the steel rod on the U-MIP. The load added to the U-MIP is divided into three classes as LL, NL and HL. The overview of the U-MIP with variable load is shown in Fig. 7(a), (b), (c). The experiments were conducted on a flat surface, 1.5 meters wide and 3 meters long, as shown in Fig. 7. (d).

First, it was applied for both NL and HL payload conditions without changing the controller parameter designed for LL. In this case, the body tilt angle of the U-MIP, which varies in the position of self-balancing, is given in figure 8(a). The most suitable FL-PI parameter for LL conditions did not give good results in the performance of the U-MIP under NL and HL conditions. The body tilt angle of the U-MIP ranged from –1.5 degrees and 1.5 degrees under LL conditions. In the NL condition, the body tilt angle ranged from –3.63 degrees to 3.27 degrees. Under HL conditions, the tilt angle changed between –5.92 degrees and 5.55 degrees. As a result, if the

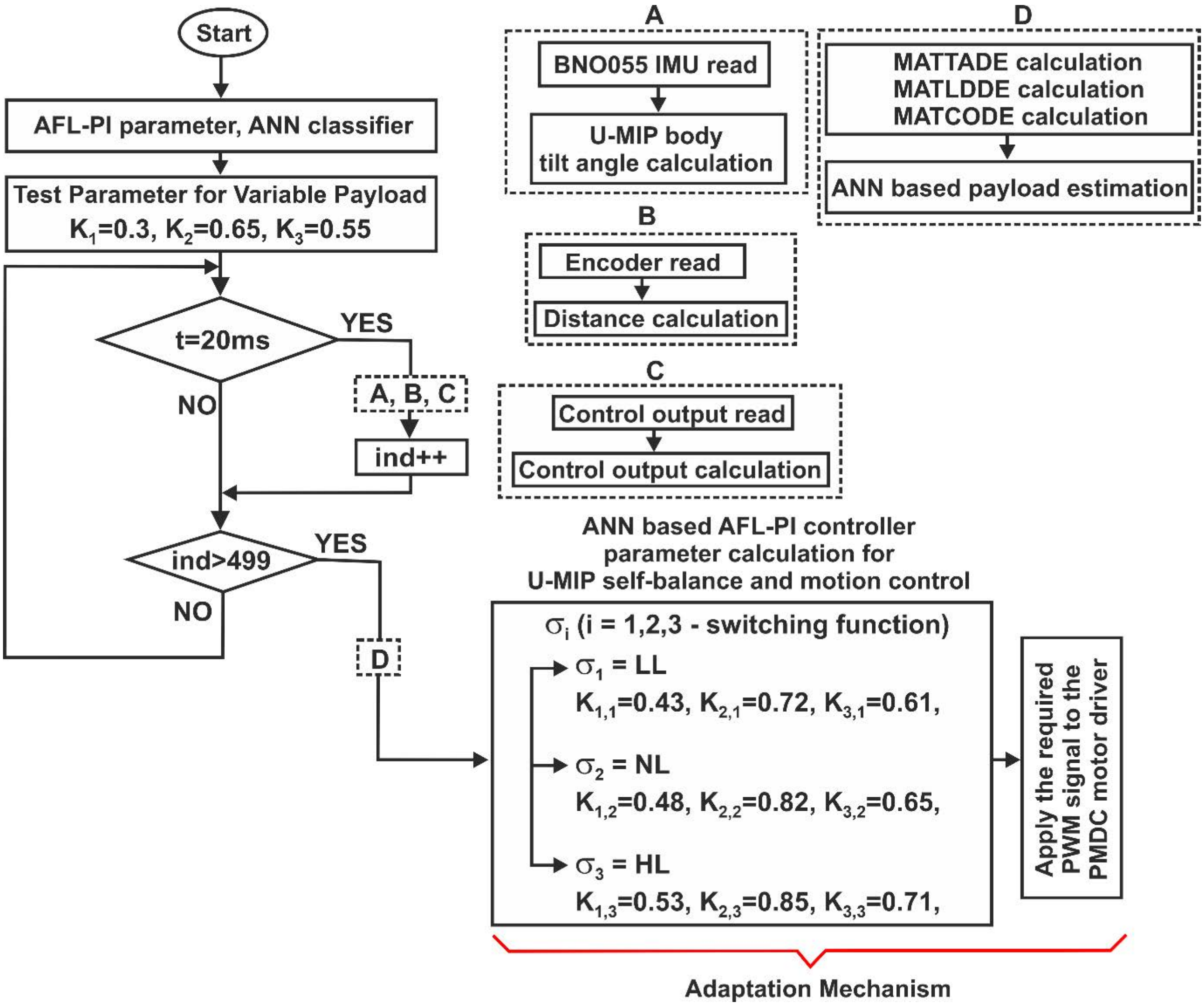

FIGURE 6. Flow diagram of the proposed novel ANN based AFL-PI adaptation mechanism.

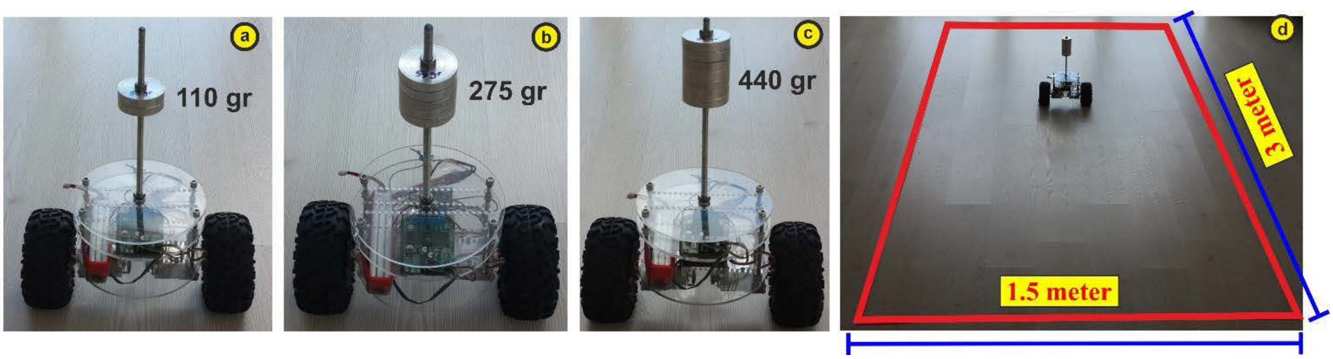

FIGURE 7. U-MIP with an added (a) 110gr payload (b) 275gr payload (c) 440gr payload (d) self-balance and motion test environment.

FL-PI controller parameters remain constant as the payload on the U-MIP increases, the value of deviation from the reference tilt angle rises significantly. Additionally, in order to the U-MIP to be able to perform different maneuvers such as forward and backward motion, right and left turns with respect to autonomous motion control, the reference body tilt angle must vary according to the payload on it. If the optimum body tilt angle value is not determined according to the payload on the U-MIP, self-balance and motion control of the robot cannot be performed. In order to better understand this situation, real-time tests were performed LL, NL and HL payload classes on the U-MIP. For the forward motion of the U-MIP, the optimum body tilt angle value determined for the LL has been applied for the HL. This situation is seen in Fig. 8(b), (c), (d). As can be seen, an unsuitable body tilt angle value leaded to an uncontrolled motion on the U-MIP. As a

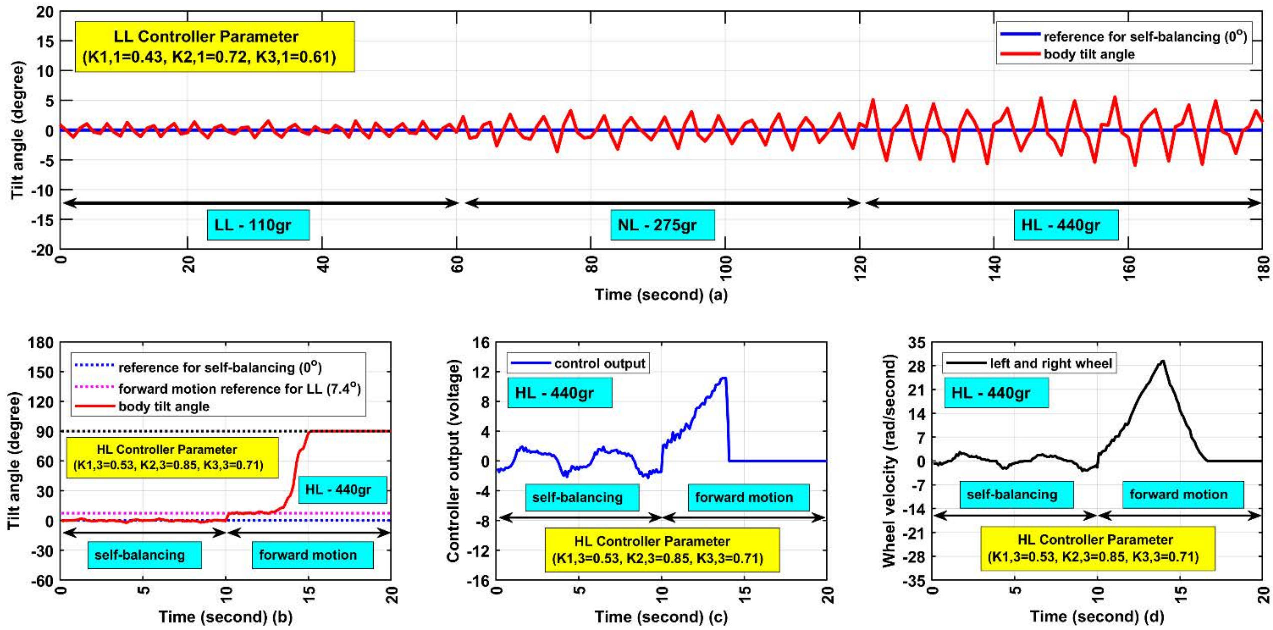

FIGURE 8. a) Response of U-MIP under NL and HL load conditions in LL controller parameter (b), (c), (d) unstable motion of U-MIP with 440gr.

result, after a certain point, the U-MIP lost its self-balance. In order to better explain the scene, the average of the data received in 0.1 seconds was taken while Fig. 8(b), (c), (d) was obtained.

In this study, a novel ML based AFL-PI controller is proposed to eliminate this negative effect due to the payload on the U-MIP. For this, it is necessary to estimate the payload class on the U-MIP. Four different type ML methods are evaluated to classify the payload. Table 5 presents the best classification results (Sensitivity (SEN), Specificity (SPE), Accuracy (ACC), F-Score) for different techniques used. SEN, SPE, ACC and F-Score equations are given as

$$\mathrm{SEN} = \frac{\mathrm{TP}}{\mathrm{TP} + \mathrm{FN}} \tag{54}$$

$$\mathrm{SPE} = \frac{\mathrm{TN}}{\mathrm{TN} + \mathrm{FP}} \tag{55}$$

$$\mathrm{ACC} = \frac{\mathrm{TP} + \mathrm{TN}}{\mathrm{TP} + \mathrm{FN} + \mathrm{TN} + \mathrm{FP}} \tag{56}$$

$$\mathrm{F}_1 - \mathrm{Score} = \frac{\mathrm{TP}}{\mathrm{TP} + \frac{1}{2}(\mathrm{FP} + \mathrm{FN})} \tag{57}$$

where TP, the number of true positives classified by the model. FN, the number of false negatives classified by the model. FP, the number of false positives classified by the model. In Table 4, ANN, k-NN, LDA and SVM based payload classification results are given according to performance criteria. For all classification methods, 10-fold cross validation was used during the training process.

During the training of ANN, the number of hidden nodes in Hidden Layer 1 (HL 1) and Hidden Layer 2 (HL 2) was increased from 10 to 100 step by 10.Here, it shows that the best classification accuracy was obtained as %98.33.

TABLE 4. Machine learning based payload classification results.

Different Type Machine Learning Classification Results				
Method	SEN	SPE	ACC	F-Score
ANN	100	96.67	98.33	98.48
k-NN	80	95	89.17	81.33
LDA	88.33	80	84.17	85.88
SVM	80	85	83.33	76.33

TABLE 5. ANN based payload classification results.

ANN Classification Results					
HL 1	HL 2	SEN	SPE	ACC	F-Score
20	10	90	90	90	89.68
20	80	90	93.33	91.67	90.98
60	70	100	96.67	98.33	98.48
70	60	96.67	90	93.33	83.86

In Table 5, the best load classifier was obtained with ANN classifier when HL 1=60 and HL 2=70.

SEN, SPE, ACC and F1-Score performance criteria were considered in evaluating the classification performance. As a result, a novel ANN based AFL-PI controller is developed to adjust the variable FL-PI controller parameters in each payload class. The system response, which includes the test parameter used to estimate the variable payloads and the optimum controller parameter that should be in the variable payload in the U-MIP, is given in the Fig. 9, 10 and 11. In the first experiment, the performance of the controller was tested

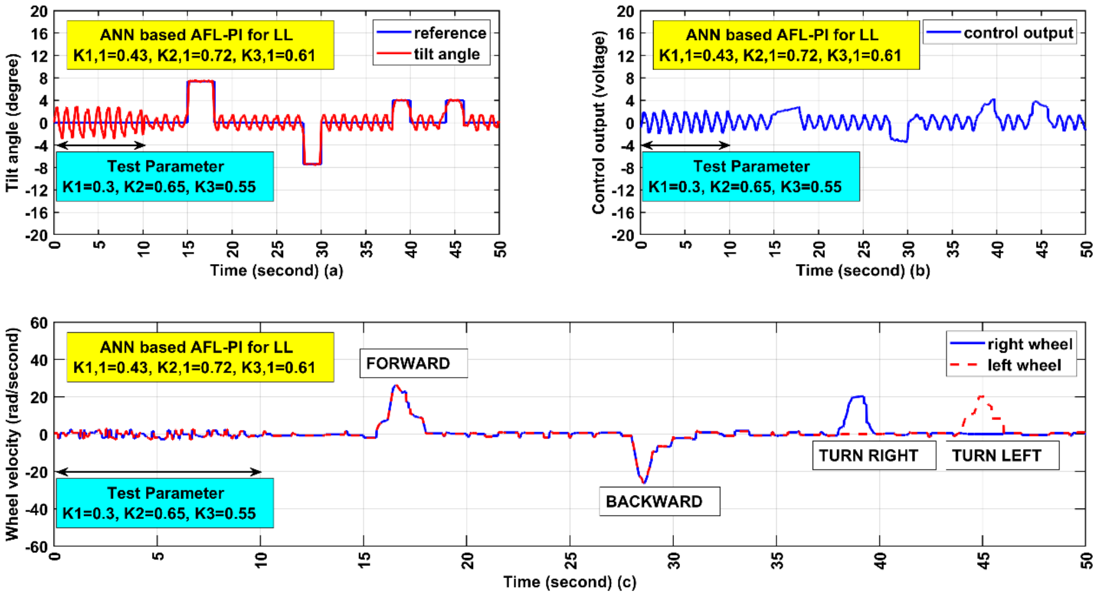

FIGURE 9. Change of data in ANN based AFL-PI controller parameter (110gr payload added).

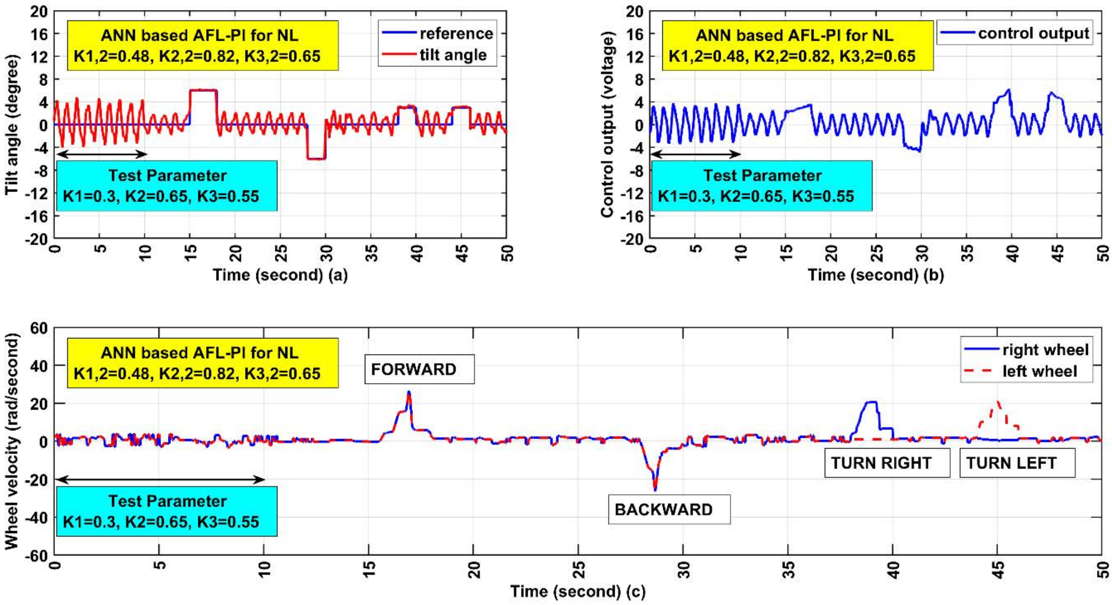

FIGURE 10. Change of data in ANN based AFL-PI controller parameter (275gr payload added).

for the references of the U-MIP body tilt angle change, wheel velocity changes and controller output change under 110gr load. The FL-PI test controller parameter and performance of the ANN based AFL-PI controller response under 110gr load conditions of the U-MIP is shown in Fig. 9. The body tilt angle changes of the U-MIP ranged from -1.5 degrees to 1.5 degrees under LL conditions. In the second case, the payload on the U-MIP was increased to 275gr. The FL-PI test controller parameter and performance of the ANN based AFL-PI controller response under 275gr payload conditions of the U-MIP is shown in Fig. 10. The body tilt angle changes of the U-MIP ranged from –2.35 degrees to 2.52 degrees under NL conditions. In the third case, the variable payload on the U-MIP was increased to 440gr. The FL-PI test controller parameter and ANN based AFL-PI controller performances of the U-MIP in this case are given in Fig. 11. The body tilt angle changes of the U-MIP ranged from –2.5 degrees to 2.59 degrees under HL conditions. However, when the FL-PI control parameters suitable for the LL condition were used in both NL and HL conditions, the body tilt angle varied considerably according to the load class. In this case, the changes of the body tilt angle of the U-MIP with time is between –3.63 degrees and 3.27 degrees for NL. For the HL, it is between –5.92 degrees and 5.55 degrees.

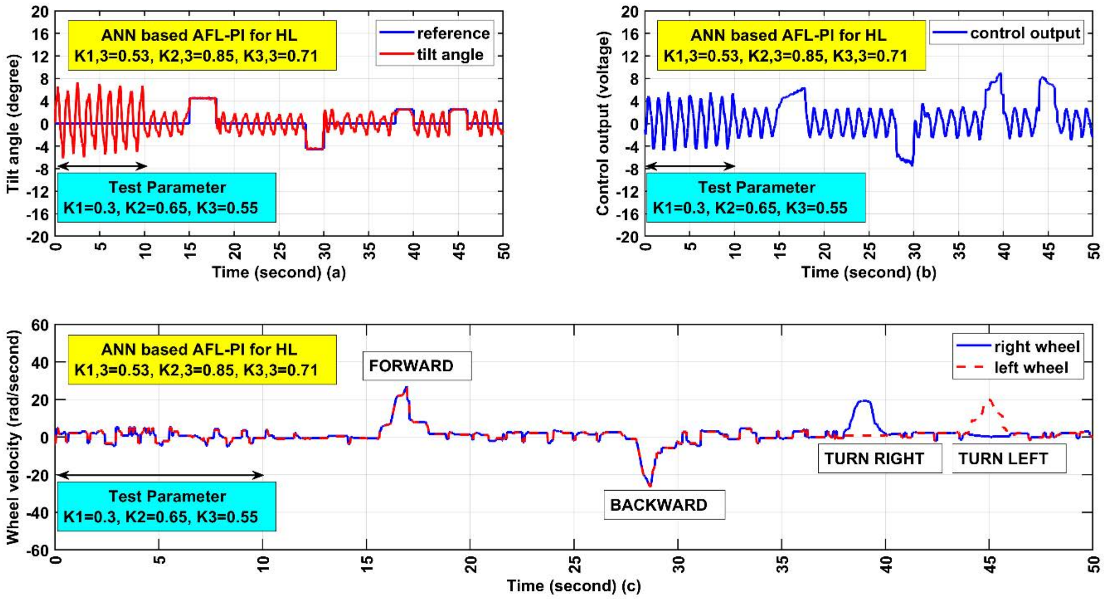

FIGURE 11. Change of data in ANN based AFL-PI controller parameter (440gr payload added).

As the payload increased, the balancing performance of the U-MIP decreased. Therefore, in order to improve the self-balance performance of the U-MIP, the robot parameters according to the payload are automatically adjusted with the ANN learning method in the AFL-PI structure. As a result, the body tilt angle change was reduced by –1.28 degrees and 0.75 degrees for NL and –3.42 degrees and 2.96 degrees for HL, respectively. The minimum and maximum body tilt angle change performance of the U-MIP robot was enhanced by %29.42 and %55.62, respectively, under NL and HL, according to the experimental results. In addition, a novel approach for motion control of U-MIP is suggested. With this proposed method, precision motion control is provided by determining the optimum reference angle values required for different maneuvers according to the variable payload on the U-MIP. The proposed ANN based AFL-PI controller is flexible to adapt to different control systems by researchers.

VI. CONCLUSION

This paper has presented a novel ANN based AFL-PI control design on a U-MIP robot with variable load. In the controller used on U-MIP, various ML based algorithms such as ANN, LDA, SVM, and k-NN are used for payload estimation. The highest payload estimation among these ML algorithms was obtained with the ANN classifier with an accuracy rate of 98.33%. Thus, ANN payload estimation algorithm was used on the U-MIP. The proposed ANN-based AFL-PI controller performs in real time on a microcontroller. Furthermore, the effectiveness of the developed ANN-based AFL-PI control method was proven by comparing it to the classical FL-PI control technique. With the proposed ANN based AFL-PI controller, the minimum and maximum body tilt angle change of U-MIP is improved by %29.42 and %55.62, respectively, in NL and HL conditions. The performance of the proposed ANN based AFL-PI controller is shown in detail in experimental results. In addition, an estimation of the payload on the robot is required for autonomous motion and performing a task. In this case, weight sensors are generally preferred. But motion control of U-MIP is not possible in case of weight sensor failure. In terms of a sensorless and low-cost solution approach, this study is very advantageous than existing methods.

REFERENCES

[1] K. He, Y. Deng, G. Wang, X. Sun, Y. Sun, and Z. Chen, "Learning-based trajectory tracking and balance control for bicycle robots with a pendulum: A Gaussian process approach," *IEEE/ASME Trans. Mechatronics*, vol. 27, no. 2, pp. 634–644, Apr. 2022.

[2] S. Wang and J. Ramos, "Dynamic locomotion teleoperation of a reduced model of a wheeled humanoid robot using a whole-body human-machine interface," *IEEE Robot. Autom. Lett.*, vol. 7, no. 2, pp. 1872–1879, Apr. 2022.

[3] C.-H. G. Li, L.-P. Zhou, and Y.-H. Chao, "Self-balancing two-wheeled robot featuring intelligent end-to-end deep visual-steering," *IEEE/ASME Trans. Mechatronics*, vol. 26, no. 5, pp. 2263–2273, Oct. 2021.

[4] S. Sekiguchi, A. Yorozu, K. Kuno, M. Okada, Y. Watanabe, and M. Takahashi, "Human-friendly control system design for two-wheeled service robot with optimal control approach," *Robot. Auton. Syst.*, vol. 131, pp. 1–16, Sep. 2020.

[5] Y. Zhang, L. Zhang, W. Wang, Y. Li, and Q. Zhang, "Design and implementation of a two-wheel and hopping robot with a linkage mechanism," *IEEE Access*, vol. 6, pp. 42422–42430, 2018.

[6] R. P. M. Chan, K. A. Stol, and C. R. Halkyard, "Review of modelling and control of two-wheeled robots," *Annu. Rev. Control*, vol. 37, no. 1, pp. 89–103, Apr. 2013.

[7] S. Kwon, S. Kim, and J. Yu, "Tilting-type balancing mobile robot platform for enhancing lateral stability," *IEEE/ASME Trans. Mechatronics*, vol. 20, no. 3, pp. 1470–1481, Jun. 2015.

[8] H.-W. Kim and S. Jung, "Fuzzy logic application to a two-wheel mobile robot for balancing control performance," *Int. J. Fuzzy Log. Intell. Syst.*, vol. 12, no. 2, pp. 154–161, Jun. 2012.

[9] V. Klemm, A. Morra, C. Salzmann, F. Tschopp, K. Bodie, L. Gulich, N. Küng, D. Mannhart, C. Pfister, M. Vierneisel, F. Weber, R. Deuber, and R. Siegwart, "Ascento: A two-wheeled jumping robot," in *Proc. 6th Int. Conf. Robot. Autom. (ICRA)*, Montreal, QC, Canada, May 2019, pp. 7515–7521.

[10] L.-G. Lin and M. Xin, "Nonlinear control of two-wheeled robot based on novel analysis and design of SDRE scheme," *IEEE Trans. Control Syst. Technol.*, vol. 28, no. 3, pp. 1140–1148, May 2020.

[11] S. Kim and S. J. Kwon, "Nonlinear optimal control design for underactuated two-wheeled inverted pendulum mobile platform," *IEEE/ASME Trans. Mechatron.*, vol. 22, no. 6, pp. 2803–2808, Dec. 2017.

[12] M. T. Watson, D. T. Gladwin, T. J. Prescott, and S. O. Conran, "Dual-mode model predictive control of an omnidirectional wheeled inverted pendulum," *IEEE/ASME Trans. Mechatronics*, vol. 24, no. 6, pp. 2964–2975, Dec. 2019.

[13] W. Ye, Z. Li, C. Yang, J. Sun, C.-Y. Su, and R. Lu, "Vision-based human tracking control of a wheeled inverted pendulum robot," *IEEE Trans. Cybern.*, vol. 46, no. 11, pp. 2423–2434, Nov. 2016.

[14] Z.-Q. Guo, J.-X. Xu, and T. H. Lee, "Design and implementation of a new sliding mode controller on an underactuated wheeled inverted pendulum," *J. Franklin Inst.*, vol. 351, no. 4, pp. 2261–2282, Apr. 2014.

[15] K. H. Su, "Adaptive fuzzy balance controller for two-wheeled robot," in *Proc. Int. Conf. Syst. Sci. Eng. (ICSSE)*, Dalian, China, Jun. 2012, pp. 30–33.

[16] J.-X. Xu, Z.-Q. Guo, and T. H. Lee, "Design and implementation of a Takagi–Sugeno-type fuzzy logic controller on a two-wheeled mobile robot," *IEEE Trans. Ind. Electron.*, vol. 60, no. 12, pp. 5717–5728, Dec. 2013.

[17] J. Huang, M. Ri, D. Wu, and S. Ri, "Interval type-2 fuzzy logic modeling and control of a mobile two-wheeled inverted pendulum," *IEEE Trans. Fuzzy Syst.*, vol. 26, no. 4, pp. 2030–2038, Aug. 2018.

[18] S. Kimura, H. Nakamura, and Y. Yamashita, "Control of two-wheeled mobile robot via homogeneous semiconcave control Lyapunov function," in *Proc. 9th IFAC Symp. Nonlinear Control Syst.*, Toulouse, France, Sep. 2013, pp. 92–97.

[19] J.-H. Hwang, Y.-C. Kang, J.-W. Park, and D. W. Kim, "Advanced interval type-2 fuzzy sliding mode control for robot manipulator," *Comput. Intell. Neurosci.*, vol. 2017, pp. 1–11, Feb. 2017.

[20] L.-X. Wang, "Stable adaptive fuzzy control of nonlinear systems," *IEEE Trans. Fuzzy Syst.*, vol. 1, no. 2, pp. 146–155, May 1993.

[21] V. Jakkula, "Tutorial on support vector machine (SVM)," School EECS, Washington State Univ., 2006, pp. 1–13, vol. 37.

[22] A. C. Müller and S. Guido, "*Introduction to Machine Learning With Python: A Guide for Data Scientists*. Sebastopol, CA, USA: O'Reilly Media, Jun. 2016.

[23] M. Paluszek and S. Thomas, *MATLAB Machine Learning Recipes: A Problem-Solution Approach*. New York, NY, USA: Apress, 2019.

[24] J. Watt, R. Borhani, and A. K. Katsaggelos, *Machine Learning Refined: Foundations, Algorithms, and Applications*. Cambridge, U.K.: Cambridge Univ. Press, 2016.

[25] D. Tomar and S. Agarwal, "A comparison on multi-class classification methods based on least squares twin support vector machine," *Knowl.-Based Syst.*, vol. 81, pp. 131–147, Jun. 2015.

[26] X.-X. Zhang, Y. Jiang, H.-X. Li, and S.-Y. Li, "SVR learning-based spatiotemporal fuzzy logic controller for nonlinear spatially distributed dynamic systems," *IEEE Trans. Neural Netw. Learn. Syst.*, vol. 24, no. 10, pp. 1635–1647, Oct. 2013.

[27] W. Pan, M. Lyu, K.-S. Hwang, M.-Y. Ju, and H. Shi, "A neuro-fuzzy visual servoing controller for an articulated manipulator," *IEEE Access*, vol. 6, pp. 3346–3357, 2018.

[28] Z. Li, Y. Zhang, and Y. Yang, "Support vector machine optimal control for mobile wheeled inverted pendulums with unmodelled dynamics," *Neurocomputing*, vol. 73, no. 13, pp. 2773–2782, 2010.

[29] M. Kok, J. D. Hol, and T. B. Schön, "Using inertial sensors for position and orientation estimation," *Found. Trends Signal Process.*, vol. 11, nos. 1–2, pp. 1–153, 2017.

[30] M. N. Armenise, C. Ciminelli, F. Dell'Olio, and V. M. Passaro, *Advances in Gyroscope Technologies*. Berlin, Germany: Springer-Verlag, 2010, pp. 1–177.

[31] *BNO055 Intelligent 9-Axis Absolute Orientation Sensor*. Accessed: Apr. 2, 2022. [Online]. Available: https://cdn-shop.adafruit.com/datasheets/BST_BNO055_DS000_12pdf

[32] A. Unluturk and O. Aydogdu, "Adaptive control of two-wheeled mobile balance robot capable to adapt different surfaces using a novel artificial neural network–based real-time switching dynamic controller," *Int. J. Adv. Robotic Syst.*, vol. 14, no. 2, pp. 1–9, Apr. 2017.

[33] Y. Yamamoto. *NXTway-GS (Self-Balancing Two-Wheeled Robot) Controller Design, MATLAB Central File Exchange*. Accessed: Jul. 18, 2022. [Online]. Available: https://www.mathworks.com/matlabcentral/fileexchange/19147-nxtway-gs-self-balancing-two-wheeled-robot-controller-design

[34] A. A. M. Habiby. *Polulu Motor Plot Generator, MATLAB Central File Exchange*. Accessed: Apr. 2, 2022. [Online]. Available: https://www.mathworks.com/matlabcentral/fileexchange/54695-polulu-motor-plot-generator

[35] J. E. Carryer, R. M. Ohline, and T. W. Kenny, *Introduction to Mechatronic Design*. Upper Saddle River, NJ, USA: Prentice-Hall, 2011, pp. 1–782.

[36] L. V. Fausett, *Fundamentals of Neural Networks: Architectures, Algorithms and Applications*. Upper Saddle River, NJ, USA: Prentice-Hall, 1994, p. 461.

[37] A. Kosarac, C. Mladjenovic, M. Zeljkovic, S. Tabakovic, and M. Knezev, "Neural-network-based approaches for optimization of machining parameters using small dataset," *Materials*, vol. 15, no. 3, pp. 1–18, Jan. 2022.

[38] T. Hastie, R. Tibshirani, and J. Friedman, *The Elements of Statistical Learning: Data Mining, Inference, and Prediction*, vol. 2. New York, NY, USA: Springer, 2009, pp. 1–745.

[39] S. Kulkarni and G. Harman, *An Elementary Introduction to Statistical Learning Theory*. Hoboken, NJ, USA: Wiley, Aug. 2011, p. 232.

[40] S. R. Kulkarni and G. Harman, "Statistical learning theory: A tutorial," *Wiley Interdiscipl. Rev., Comput. Statist.*, vol. 3, no. 6, pp. 543–556, 2011.

[41] H. Liu and S. Zhang, "Noisy data elimination using mutual k-nearest neighbor for classification mining," *J. Syst. Softw.*, vol. 85, no. 5, pp. 1067–1074, May 2012.

[42] I. H. Witten, E. Frank, M. A. Hall, and C. J. Pal, *Data Mining: Practical Machine Learning Tools and Techniques*, 4th ed. San Mateo, CA, USA: Morgan Kaufmann, Oct. 2016, p. 633.

ALI UNLUTURK was born in Konya, Turkey, in 1983. He received the M.S. and Ph.D. degrees in electrical and electronics engineering from Selçuk Üniversitesi, Konya, in 2012 and 2017, respectively. From 2008 to 2009, he worked as an Engineer at the Transmission Unit, Türk Telekom Company, Turkey. From 2009 to 2012, he worked as an Electrical and Electronics Engineer at government institution. In government institution, he had the opportunity to carry out projects with defense industry companies, such as ASELSAN. From 2012 to 2017, he worked as a Research Assistant at the Department of Electrical and Electronics Engineering, Selçuk Üniversitesi. Since 2017, he has been working as an Assistant Professor with the Electrical and Electronics Engineering Department, Erzurum Technical University, Erzurum. His research interests include control theory, adaptive control systems, fuzzy logic control, real-time control and applications, and renewable energy systems.

OMER AYDOGDU was born in Konya, Turkey, in 1973. He received the B.S., M.S., and Ph.D. degrees in electrical and electronics engineering from Selçuk Üniversitesi, Konya, in 1995, 1999, and 2006, respectively. From 1996 to 2007, he was a Research Assistant with the Department of Electrical and Electronics Engineering, Selçuk Üniversitesi. From 2007 to 2018, he worked as an Assistant Professor and an Associate Professor with the Department of Electrical and Electronics Engineering, Selçuk Üniversitesi. From 2018 to 2020, he worked as an Associate Professor with the Department of Electrical and Electronics Engineering, Konya Technical University, Konya, where he has been a Professor, since 2020. He is the author of a book chapter and more than 70 scientific publications. His research interests include control theory, adaptive control systems, fractional order control, fuzzy logic control and applications, and brushless dc motors and drives.